S. D. Bellows and T. W. Leishman, "Acoustic source centering of musical instrument directivities using acoustical holography", in Proceedings of meetings on acoustics, Vol. 42, 1 (2020), p. 055002

and may be found at https://doi.org/10.1121/2.0001371

Volume 42 http://acousticalsociety.org/

179th Meeting of the Acoustical Society of America

Acoustics Virtually Everywhere

7-11 December 2020

Signal Processing in Acoustics: Paper 5aSPb4

Acoustic source centering of musical instrument directivities using acoustical holography

Samuel D. Bellows and Timothy W. Leishman
Department of Physics and Astronomy, Brigham Young University, Provo, UT, 84602; samuel.bellows11@gmail.com; twleishman@byu.edu

The acoustic center of a source is commonly defined as the point from which spherical wavefronts appear to diverge. Measuring directivities of sound sources with a surrounding spherical array whose geometric origin is not aligned with the acoustic center of the source can lead to distortions in directivity patterns. Thus, a method is desired to obtain both the far-field directivity pattern and to determine the acoustic center of a source. This work illustrates how acoustical holography can identify the reference frame from which spherical waves diverge by studying various musical instruments' acoustic centers.

Published by the Acoustical Society of America

 https://doi.org/10.1121/2.0001371

1. INTRODUCTION

Directivity measurements characterize radiation of sound sources while providing valuable information for many applications, such as room-acoustic simulations and auralizations. In many cases, a surrounding spherical microphone array assesses directivity. However, a practical question regards the proper positioning of a sound source relative to the array. It seems logical to align the array's geometric center with the source's acoustic center, sometimes defined as the point from which spherical waves appear to diverge. This work explores relevant source placement issues and presents an algorithm for detecting the source's acoustic center.

2. DIRECTIVITY MEASUREMENTS

Figure 1 shows an array used to measure the directivities of 16 musical instruments and speech. The microphones of the fixed arc captured a semicircular slice of a measurement sphere with 5° polar-angle increments. Progressive 5° azimuthal rotations of the repeating sound source yielded a full spherical measurement with polar and azimuthal resolutions suggested by an AES standard for loudspeaker directivity measurements.[1] A frequency response function (FRF) technique compensated for amplitude and spectral variations between the incremental rotations. The three plots in Fig. 2(a) show the raw autospectral balloons measured by the array for a bassoon note A2 fundamental (110 Hz) and two additional partials. Those in Fig. 2(b) show the raw FRF data with no smoothing or interpolating effects. The latter illustrate how the FRF method alone compensates significantly for rotational measurement variations at these frequencies. Despite these benefits, the directivity effects of the source position relative to the array geometry remain unresolved. The following sections treat this matter in greater detail.

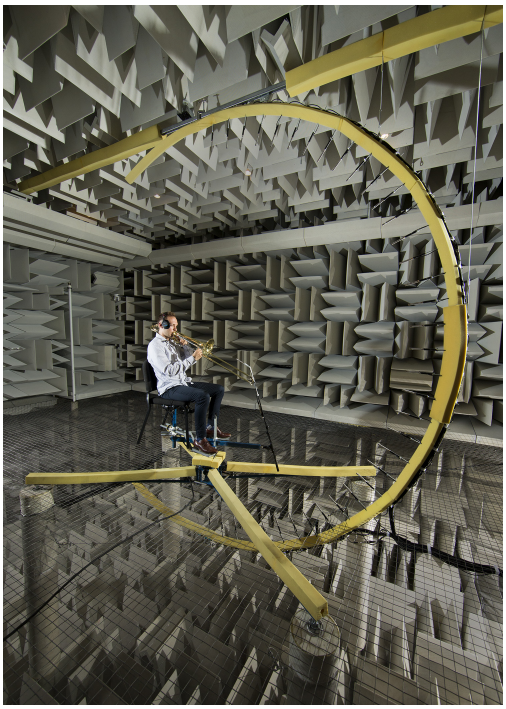

Figure 1: Microphone array used to measure the directivities of 16 musical instruments and speech.

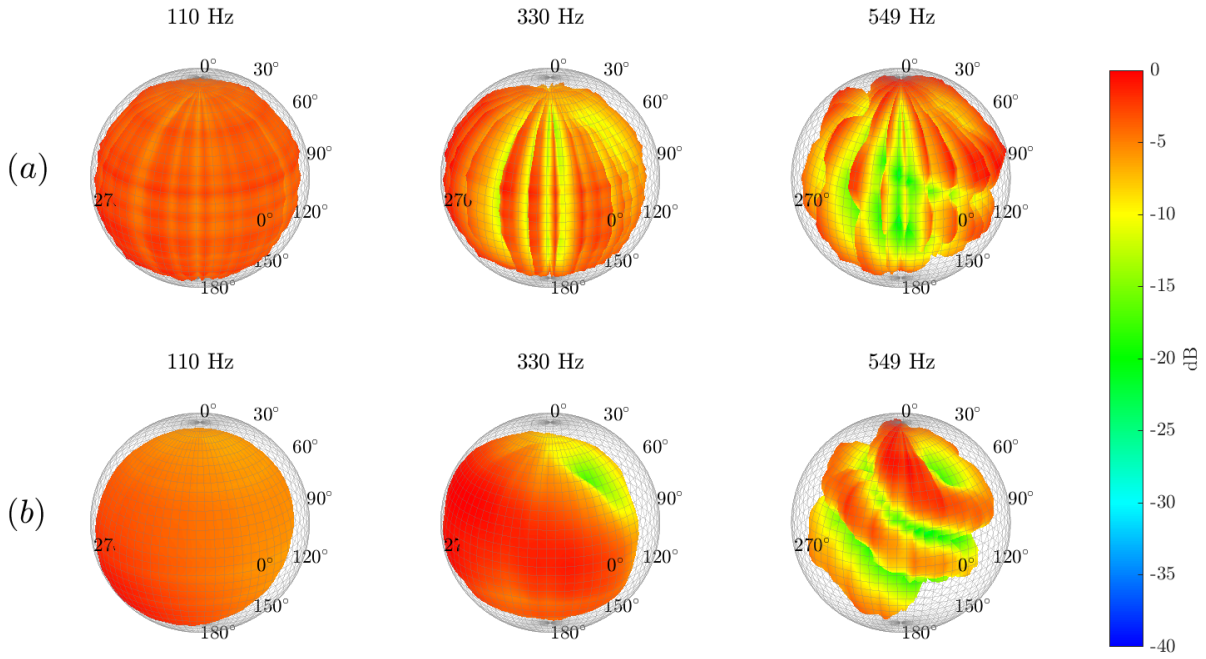

Figure 2: Illustration of the benefits of the FRF compensation method for measured bassoon directivity. (a) Array autospectral balloons for the note A2 fundamental (110 Hz), third harmonic (330 Hz), and fifth harmonic (549 Hz). (b) The FRF balloons for the same narrowband partials. All balloons are plotted on a 40 dB scale relative to the maximum value.

3. THEORY

The Helmholtz equation and its far-field pressure solution form the foundation for understanding of the effects of misalignment between the geometric and acoustic centers of a source in directivity measurements. It also leads to the development of an algorithm to identify the acoustic center of the source.

A. HELMHOLTZ EQUATION SOLUTION

The exterior solution to the Helmholtz equation in spherical coordinates has the form[2]

$$p(r,\theta,\phi,k) = \sum_{n=0}^{\infty} \sum_{m=-n}^{n} c_n^m(k) h_n^{(2)}(kr) Y_n^m(\theta,\phi), \qquad r \geq a, \tag{1}$$

where $p(r,\theta,\phi,k)$ is the pressure, $h_n^{(2)}(kr)$ are the spherical Hankel functions of the second kind (for outgoing waves with $e^{i\omega t}$ time dependence) of order n, and $Y_n^m(\theta,\phi)$ are the spherical harmonics of degree n and order m.[3] With the pressure measured at the boundary surface $r = a$, Eq. (1) is valid on the domain $r \geq a$. To calculate the pressure expansion coefficients $c_n^m(k)$ from the measured pressure, an exploitation of the orthogonality of the spherical harmonics yields

$$c_n^m(k) = \frac{1}{h_n^{(2)}(ka)} \int_0^{2\pi} \int_0^{\pi} p(a,\theta,\phi,k), \overline{Y_n^m(\theta,\phi)} \sin\theta d\theta d\phi, \tag{2}$$

where the overbar denotes complex conjugation.

In practice, a discrete spherical sampling scheme is useful to compute the spherical harmonic expansion only to a certain degree *N*. Because higher frequencies tend to require more higher-degree terms, the number of sampling positions must allow the expansion to converge correctly to the measured data while minimizing spatial aliasing. For this work, Chebyshev quadrature weights developed previously[4] enabled the numerical calculation of the integral over the sphere. Figure 3 illustrates the measured cello FRF balloon for the note F3 at 523 Hz (1 Hz resolution) and compares it to the balloons of its spherical harmonic expansions for several maximum degrees *N*. The expansion converges to the measured pressure with the inclusion of enough higher-degree terms while also providing some degree of smoothing.

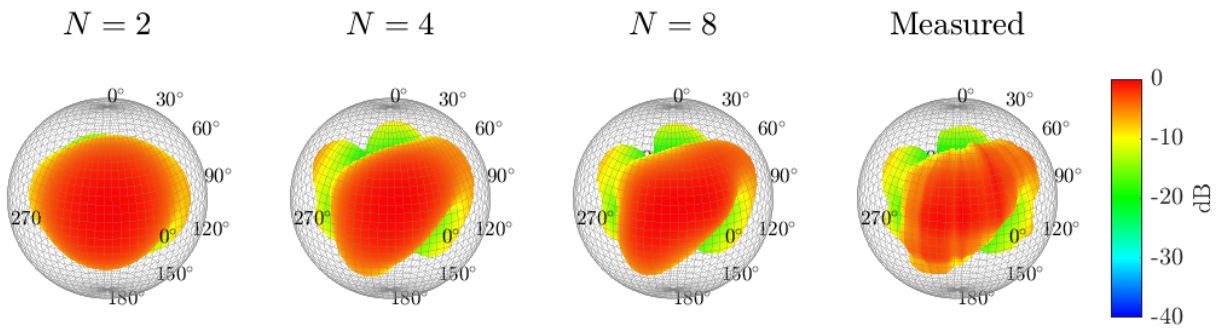

Figure 3: Spherical harmonic expansion of cello directivity at 523 Hz (3rd harmonic of F3) with increasing maximal expansion degree N, as compared to the raw measured result.

B. FAR-FIELD

However complex wave propagation may be in the far-field, it is well-approximated by a simple spherical outgoing wave multiplied by an angular directivity function that remains consistent with increasing radius r. There are two general conditions for predicting whether the radius is sufficiently far from the radiating body to be in the far-field. The first is the acoustic condition, in which the observation radius is much greater than the wavelength: $r >> \lambda \implies kr >> 1$. The second is the geometric condition, requiring that the observation radius is much greater than the characteristic source dimension, including any surrounding diffracting body: $r >> d$.

By applying the large-argument relation of the spherical Hankel functions,

$$h_n^{(2)}(kr) \approx i^{n+1}\frac{e^{-ikr}}{kr}, \qquad kr >> 1, \tag{3}$$

one finds that the the far-field pressure is the product of a spherical wave and an angular directivity function:

$$p(r,\theta,\phi,k) \approx \frac{e^{-ikr}}{kr}\sum_{n=0}^{\infty}\sum_{m=-n}^{n} c_n^m(k) i^{n+1} Y_n^m(\theta,\phi). \tag{4}$$

The unnormalized far-field directivity function $\tilde{D}_\infty(\theta,\phi,k)$ is then

$$\tilde{D}_\infty(\theta,\phi,k) = \sum_{n=0}^{\infty}\sum_{m=-n}^{n} c_n^m(k) i^{n+1} Y_n^m(\theta,\phi). \tag{5}$$

Figure 4 illustrates these concepts for a theoretical model of a radially vibrating cap on a rigid sphere of radius a with cap radius $a_c = 0.31a$ and wavenumber $k = 5$. As the increase of observation radius r causes $kr >> 1$, the normalized directivity beam pattern $B_\infty(\theta,\phi,k) = 20\log|D_\infty(\theta,\phi,k)|$ converges to the far-field pattern, becoming invariant to further increases in r.

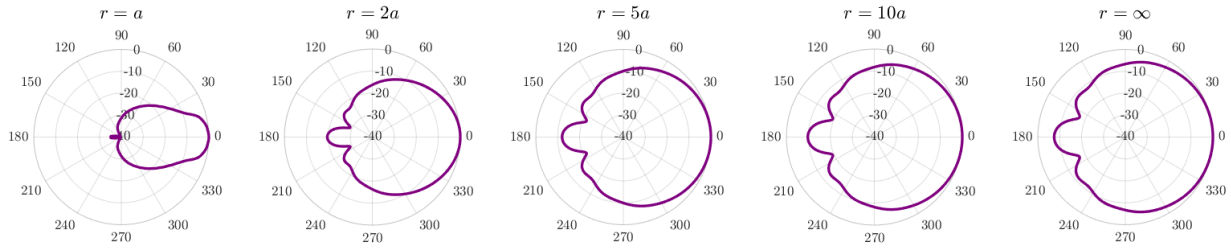

Figure 4: Normalized directivity beam pattern of a vibrating cap on sphere with increasing measurement radius r. The polar plots are all on a 40 dB scale.

C. ACOUSTIC CENTER

The far-field nature of all spherically diverging waves motivates the concept of an acoustic center. While the latter has been defined in different ways, such as the point from which spherical waves seem to diverge or the point from which the pressure varies with inverse proportion to the distance,[5] it carries a general connotation that because the complex radiation pattern simplifies to a spherically diverging wave, there must be an associated center of that wave. The applications for acoustic centering are many, including calculating transducer sensitivities[6] or evaluating anechoic properties of rooms.[7] However, past research has shown that an acoustic center is not only frequency dependent, but its actual position may vary depending on which definition is used.[8] It may also depend upon the changing characteristics of a distributed source, such as a played musical instrument.

D. DIRECTIVITY PRODUCT THEOREM

This section will develop the relationship between an acoustically centered directivity pattern and an uncentered directivity pattern. The free-space Green's function

$$G_k(\mathbf{r}|\mathbf{r}_0) = \frac{e^{-ik|\mathbf{r}-\mathbf{r_0}|}}{4\pi|\mathbf{r}-\mathbf{r_0}|} \tag{6}$$

is the solution to the Helmholtz equation for a unit-amplitude point source at position $\mathbf{r}_0$ and behaves as the system's spatial impulse response. By application of the first directivity product theorem,[2] the far-field pressure observed in a coordinate frame whose origin is displaced from the acoustic center by $\mathbf{r}_c$ is

$$p_\infty(\theta, \phi, k) \propto G_k(\mathbf{r}|\mathbf{r}_c) D_{\infty,c}(\theta, \phi, k), \tag{7}$$

where $D_{\infty,c}$ is the far-field directy pattern of the source in the centered coordinate frame. In other words, the measured far-field pressure is simply the far-field directivity pattern in the centered frame imposed on an outgoing spherical wave originating from $\mathbf{r}_c$. Furthermore, to be in the geometric far-field, the observation distance r should be much greater than r_c, in which case the magnitude of the free-space Green's function loses its angular dependance:

$$|G_k(\mathbf{r}|\mathbf{r}_c)| \approx \frac{1}{4\pi r}. \tag{8}$$

Consequently, in the far-field, the magnitudes of the normalized far-field directivity patterns in the centered and uncentered frames must be equivalent:

$$|D_{c,\infty}(\theta, \phi, k)| = |D_\infty(\theta, \phi, k)|. \tag{9}$$

This result is also apparent as one considers the measurement of a source with a large spherical array of infinite diameter, where the relative shift between the source acoustic center and the array geometric center becomes negligible. It is of note that while the far-field magnitude patterns are equal, there is a relative phase shift $-ik|\mathbf{r} - \mathbf{r_c}|$ in the far-field phase patterns caused by the difference in observation frames.

Figure 5 illustrates the effect for the directivity patterns of a centered quadrupole and an uncentered quadrupole. In both cases, an $a = 1$ m array first measures the field pressure before computation of the expansion coefficients; for the centered case, the quadrupole is located at the origin, whereas for the uncentered case, the quadrupole is positioned at $(x, y, z) = (0.7, 0, 0)$ m. Arrays with increasing radii of 2 and 10 m then evaluate the pressure using Eq. (1). Finally, calculation of the far-field directivity pattern follows from Eq. (5). The various plots demonstrate that the directivity patterns of the centered and uncentered sources are the same in the far field.

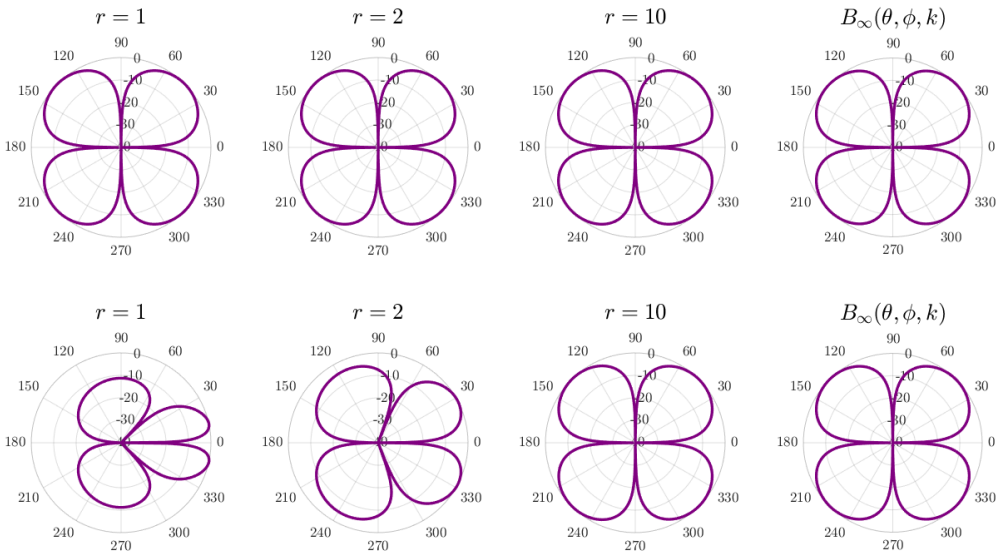

Figure 5: Directivity beam patterns of a centered and uncentered quadrupole, measured with increasing observation radius, plotted on a 40 dB scale. Top row: Polar directivity beam pattern of the centered quadrupole measured at various radii and the far-field pattern. Bottom row: Directivity beam pattern the uncentered quadrupole measured at the same radii and at the far field.

Many previous works have justified the need for acoustic source centering because measured uncentered directivity patterns show distortions or differ from theoretical or assumed far-field patterns.[9] However, if only magnitude far-field data is required, such as in $1/n$-octave-band data for room-acoustic simulations or auralizations, a far-field pressure expansion suffices. Furthermore, it is evident that the phase shift $-ik|\mathbf{r} - \mathbf{r_c}|$ between the centered and uncentered patterns accounts for the difference between the geometric and acoustic centers. Consequently, in acoustic simulations, if complex directivity data is necessary and a geometric source positioning scheme is more straightforward to use than an acoustic positioning scheme, a complex-valued far-field pattern in the uncentered frame remains beneficial. While for some applications uncentered but geometrically fixed directivities may be preferred, there are other circumstances wherein it might be beneficial to know the acoustic center of a source, such as when seeking theoretical insights about the source or implementing practical sampling considerations. The following section develops an acoustic source-centering algorithm to satisfy this need.

4. CENTERING ALGORITHM

The equal far-field magnitude directivity patterns of the centered and uncentered reference frames are amenable to further exploitation because they circumvent mutable assumptions about centered directivity patterns that can cause existing centering algorithms to fail. For the proposed centering method, one may consider that for a given wavenumber k, a radiating object has an acoustic center at origin O_c, falling at $\mathbf{r}_c$ from the uncentered measurement reference frame origin O [see Fig. 6(a)]. One may then assume that at some radius b, as measured from the acoustic center, the observed directivity pattern magnitude, with its spherically diverging wavefronts centered on O_c, has adequately converged to the far-field pattern of the source. This directivity pattern will then be nearly invariant to further increases in observation radius as measured from the centered origin O_c, as discussed in Sec. 3.2. The pattern detected on an evaluation sphere, whose center is not aligned with the acoustic center, generally exhibits distortion because it cuts through the acoustically centered, spherically diverging wavefronts. Finding the reference frame that exhibits the least distortion between the known far-field pattern and that evaluated on a sphere of radius $R > b$ is tantamount to finding the reference frame best aligned with the spherically diverging wavefronts from the source acoustic center, and consequently the reference frame whose origin is the acoustic center.

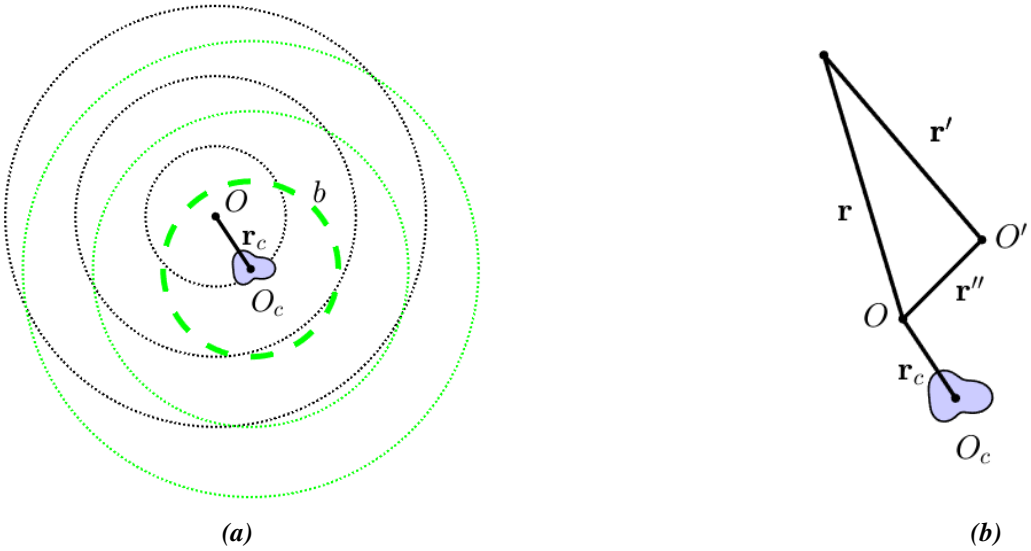

Figure 6: Geometric illustrations for the proposed centering algorithm. (a) The measurement origin is O and the corresponding spherical wavefronts centered about this origin appear as black dotted circles. The acoustic center of the radiating body is O_c and the spherical wavefronts centered about this origin appear as green dotted lines. The sphere of radius b centered about O_c and shown as a green dashed circle represents the distance prescribed by the far-field relations to ensure that the directivity pattern in the centered frame has adequately converged to its far-field pattern. (b) A reference diagram for the position vectors relating the original measurement origin O, the acoustic center O_c, and the trial frame origin O'.

The calculation of $|D_\infty(\theta, \phi, k)|$ is the first step to determine the source's acoustic center and will serve as the reference pattern to compare directivities of different frames. It follows from evaluating Eq. (5) once the expansion coefficients $c_n^m(k)$ have been determined. Next, one may create a new trial coordinate frame with origin O' at position $\mathbf{r}''$ and a relative observation position at $\mathbf{r}' = (r', \theta', \phi')$, as shown in Fig. 6(b). In this trial frame, one evaluates the pressure on a sphere of constant radius $r' = R$ using Eq. (1). While this evaluation sphere must completely enclose the original measurement sphere of radius a for Eq. (1) to

remain valid, the observation radius R would be sufficiently large in practice to also satisfy the condition that the observed pressure is in the far-field by enclosing the sphere of radius b centered about the acoustic center $\mathbf{r}_c$. Calculation of the normalized directivity $D(r', \theta', \phi')$ in this reference frame then follows from the measured pressure. The acoustic center subsequently can be determined as the origin $\mathbf{r}''$ that minimizes the difference between the known far-field pattern and the measured pattern on the spherical wavefront in the trial frame. This minimizes the cost function $J(\mathbf{r}'')$, where the deviation between the directivity patterns is in a least-squares sense:

$$J(\mathbf{r}'') = \|D(R, \theta', \phi', k) - D_\infty(\theta, \phi, k)\|_2^2. \tag{10}$$

Figure 7 gives a simple example for the case of a point source. In the diagram of Fig 7(a), a 1 m radius array measures the pressure produced by a monopole at $\mathbf{r} = (0.7, 0, 0)$ m. A cross-section of the spherical measurement array appears as black dots and the monopole position appears as a red $\times$. Figure 7(b) shows the measured directivity balloon that lacks expected spherical symmetry. However, reconstruction using measurement positions shown as green dots in Fig. 7(a) produces the valid omnidirectional spherical wavefront from the (known) acoustic center.

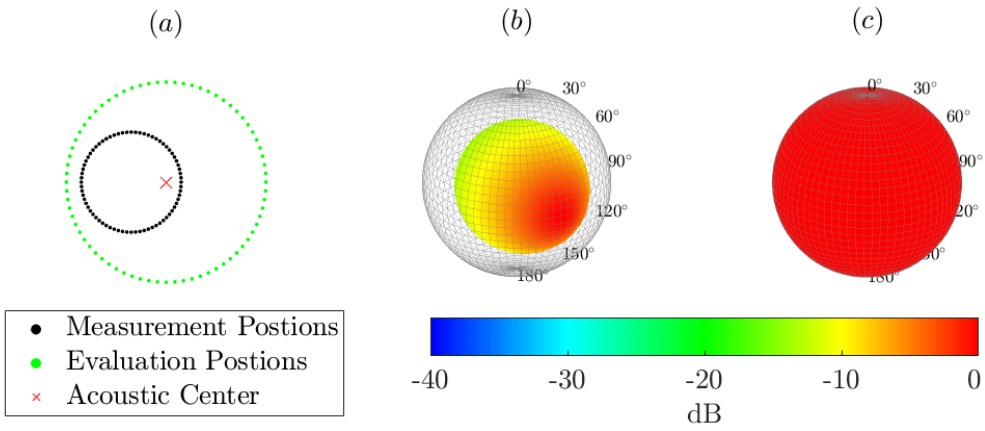

Figure 7: Simple illustration of the centering algorithm. (a) A diagram of the original measurement sampling positions (black dots), acoustic center (red $\times$), and evaluation points (green dots). (b) The directivity of the uncentered monopole as determined by the measurement array. (c) The directivity of an acoustically centered monopole as seen by the evaluation array.

5. RESULTS

A. MULTIPOLE SOURCES

The algorithm was tested on sources with known acoustic centers: a monopole, dipole, and quadrupole, each displaced some distance along the x-axis and measured with a spherical array of 1 m radius. The algorithm performed a global search to find the minimum deviation from the far-field pattern computed from the expansion coefficients. The surfaces of the objective functions in the x-y plane appear in Fig. 8. In all cases, the minimum of the objective function gives the correct acoustic center, regardless of the magnitude of the displacement or the source's frequency. Furthermore, the objective functions over this range all appear to be convex.

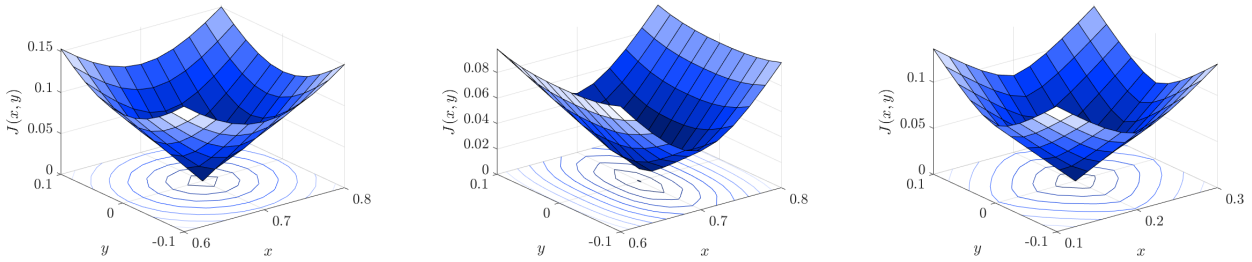

Figure 8: Objective functions for a monopole, dipole, and quadrupole, each with known acoustic centers. (a) Error functional for monopole at 1 kHz and coordinates (0.7, 0, 0). (b) Error functional for a dipole at 1 kHz and coordinates (0.7, 0, 0). (c) Error functional for quadrupole at 5 kHz and coordinates (0.2, 0, 0).

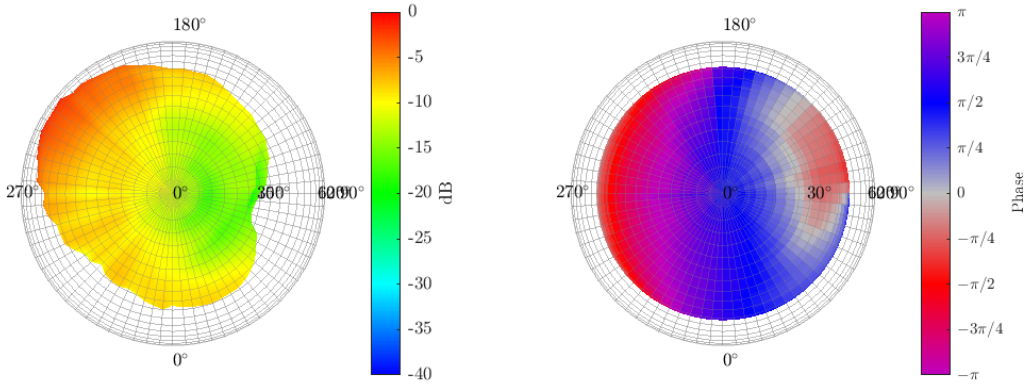

Figure 9: Magnitude and phase balloons for a French Horn at 550 Hz.

.

B. MUSICAL INSTRUMENTS

This section presents selected directivity results for various musical instruments. The instruments were measured with the array shown in Fig. 1, and the pressure was calculated using a frequency response technique.[10]

i. French Horn

Figure 9 shows the magnitude and phase balloons measured from a French horn at 550 Hz, the fifth harmonic of the note A2, and radius 1.83 m, from a vantage point directly above the instrument. The hornist faced azimuthally toward 0°. The resultant directivity balloon appears in Fig. 10(a), with expansion coefficients computed to degree $N = 5$. The source centering algorithm identified the acoustic center at $(x, y, z) = (-0.11, -0.31, -0.14)$ m, which subsequently resulted in the centered balloon of Fig. 10(b). For reference, the far-field directivity pattern for this frequency appears in Fig. 10(c). Finally, cross-sections of the objective function $J(\mathbf{r}'')$ appear in Fig. 11. Over the range shown, the objective function remains convex.

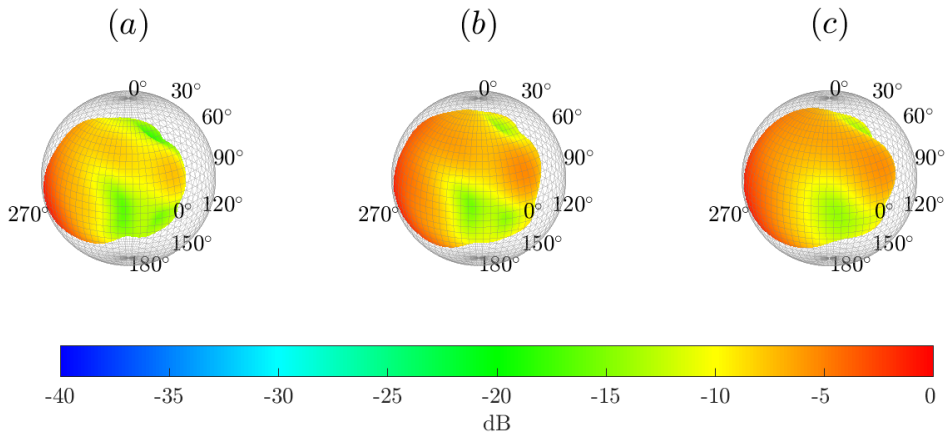

Figure 10: Acoustic source centering of a french horn at 550 Hz. (a) Measured directivity balloon. (b) Centered directivity balloon. (c) Far-field directivity balloon.

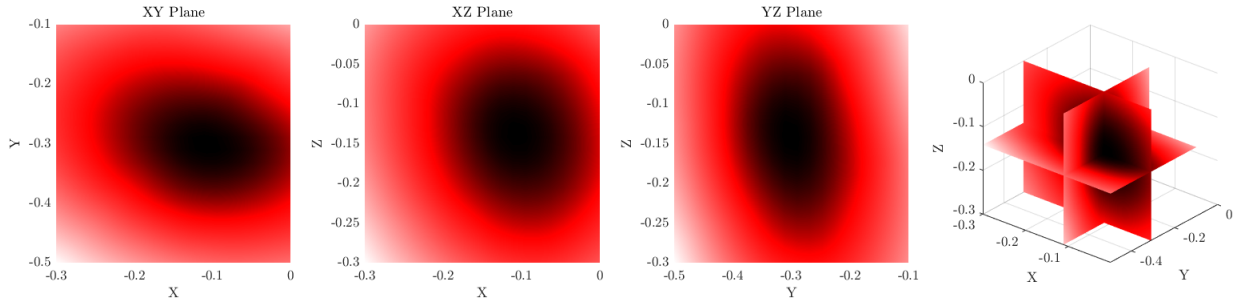

Figure 11: Objective function $J(\mathbf{r}'')$ for the acoustic centering of a french horn at 550 Hz.

ii. Flute

Figure 12 shows similar results for the flute at 621 Hz, the fundamental frequency for E♭5. Figure 12(a) shows an $N = 8$ degree expansion of the measured pressure, Fig. 12(b) shows the centered directivity, and Fig. 12(c) shows the reference far-field directivity. The acoustic center was identified to be $(x, y, z) = (-0.14, -0.19, -0.14)$ m, with the objective function for this frequency appearing in Fig. 13.

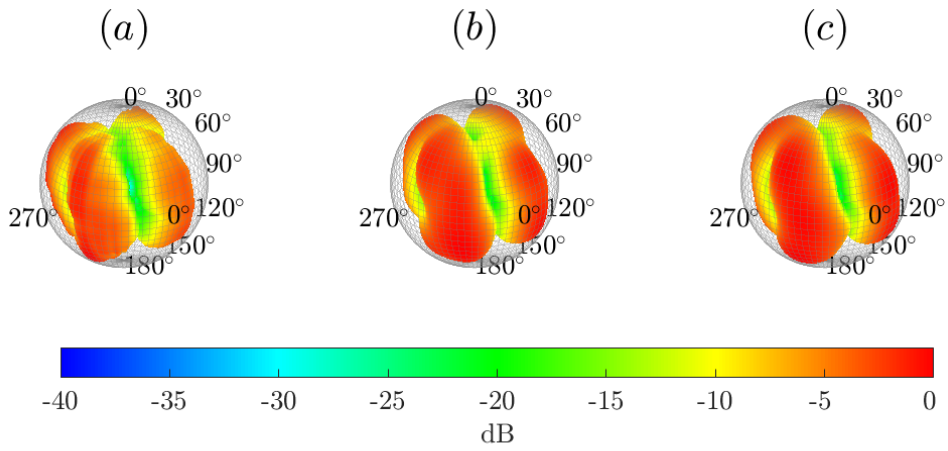

Figure 12: Acoustic source centering of a played flute at 621 Hz. (a) Measured directivity balloon. (b) Centered directivity balloon. (c) Far-field directivity pattern.

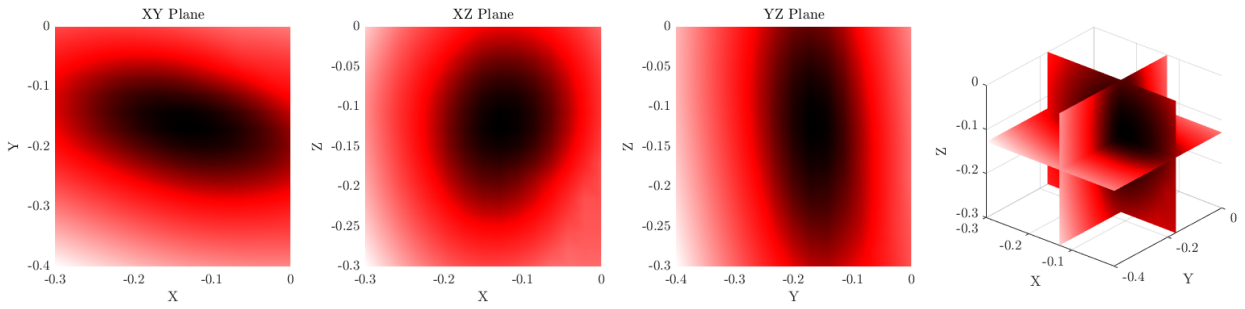

Figure 13: Objective function $J(\mathbf{r}'')$ for the acoustic centering of a flute at 621 Hz.

6. CONCLUSIONS

The acoustic center of a source is important in directivity measurements. Because the far-field magnitude pattern is the same whether the source acoustic center and array geometric center coincide or not, one should generally propagate the pressure adequately to the far field, which may require relatively high sampling density to accurately represent the magnitude and phase of the pressure at desired frequencies. To determine the source acoustic center, one may employ an algorithm based on spherical-wavefront alignment. This work has presented the approach and shown that the objective function surface is convex for the tested sources

over a limited bandwidth. Future work includes studying the algorithm for a wider variety of sources and bandwidths to improve the method's robustness.

ACKNOWLEDGMENTS

This work was funded by the William James Strong and Charlene Fuhriman Strong Family Musical Acoustics Endowed Fellowship Fund, and the Institute for Scientific Research in Music.

REFERENCES

[1] Audio Engineering Society AES56-2008 (r2019), "AES standard on acoustics - Sound source modeling - Loudspeaker polar radiation measurements," New York, 2019.

[2] E. G. Williams, *Fourier Acoustics: Sound Radiation and Nearfield Acoustical Holography*. London: Academic Press, 1999.

[3] T. M. Dunster, *NIST Handbook of Mathematical Functions*. New York: Cambridge University Press, 2010.

[4] S. D. Bellows and T. W. Leishman, "Spherical harmonic expansions of high-resolution musical instrument directivities," *Proc. Mtgs. Acoust. 35, 035005*, 2018.

[5] American National Standard ANSI S1.1-1994 (r2004), "Acoustical Terminology," March 2004.

[6] International Electrotechnical Commission (IEC), "Electroacoustics-measurement microphones-part 3: Primary method for free-field calibration of laboratory standard microphones by the reciprocity technique" June 2016.

[7] K. A. Cunefare, V. B. Biesel, J. Tran, R. Rye, A. Graf, M. Holdhusen, and A.-M. Albanese, "Anechoic chamber qualification: Traverse method, inverse square law analysis method, and nature of test signal," *The Journal of the Acoustical Society of America*, vol. 113, no. 2, pp. 881–892, 2003.

[8] F. Jacobsen, S. B. Figueroa, and K. Rassmussen, "A note on the concept of acoustic center," *Journal of the Acoustical Society of America*, vol. 115, no. 4 pp. 1468 – 1473, 2004.

[9] I. Ben Hagai, M. Pollow, M. Vorländer, and B. Rafaely, "Acoustic centering of sources measured by surrounding spherical microphone arrays," *The Journal of the Acoustical Society of America*, vol. 130, no. 4, pp. 2003–2015, 2011.

[10] K. J. Bodon, "Development, evaluation, and validation of a high-resolution directivity measurement system for played musical instruments," Master's thesis, Brigham Young University, 2016.